PERGAMON

International Journal of Heat and Mass Transfer 42 (1999) 3815–3829

International Journal of HEAT and MASS TRANSFER

www.elsevier.com/locate/ijhmt

Thermal patterns on the smooth and rough walls in turbulent flows

G. Hetsroni*, A. Mosyak, R. Rozenblit, L.P. Yarin

Technion—Israel Institute of Technology, Department of Mechanical Engineering, 32 000 Haifa, Israel

Received 20 May 1998; received in revised form 12 January 1999

Abstract

Here an experimental study of temperature fields on the surface of smooth and rough walls is dealt with, in turbulent channel and pipe flows. The hot-foil infrared technique was used to measure the local (instantaneous and time average) temperatures on the walls. The detailed data on mean and fluctuation temperature distributions are presented. The temperature fields in the vicinity of a single macroscale roughness (particle) as well as a lattice of particles are studied.

1. Introduction

Heat transfer in turbulent flows over smooth walls has attracted the attention of numerous investigators during the last decades. The results of some researches devoted to this problem are summarized in monographs and textbooks [1–3]. Also, heat transfer in turbulent flows over rough surfaces has been extensively studied. It was shown that these surfaces enhance heat transfer from the wall to the fluid and raise the heat transfer coefficient [4,5].

At present there are a number of publications dealing with the effect of ribs, coarse particles etc. on the convective heat transfer in turbulent flows [6–13]. These contain, mainly, data related to the mean characteristics of the flow. This does not allow one to estimate the specific features of the heat transfer in the immediate neighbourhood of the wall. For better understanding of the real mechanism of heat transfer from the smooth and rough walls to a fluid, detailed studies of the temperature fields on the walls are needed.

The study of temperature fluctuations on the wall presents a special interest. It is necessary to estimate the effect of turbulence on durability of heated wall lifetime (considering fatigue of material, etc.) as well as to provide correct formulation of thermal boundary conditions to calculate heat transfer in turbulent boundary layer.

The effect of temperature fluctuations on the wall on thermal structure of turbulent boundary layer was investigated numerically by Kasagi et al. [14] and Sommer et al. [15]. It was shown that the wall temperature fluctuations significantly affect temperature field up to $y^+ \simeq 30$, i.e. within the region determining scalar transfer. However, at present, the detailed experimental data regarding temperature field on the wall are limited. In particular, there are no data about temperature fluctuations on the rough walls, effect of Reynolds number on statistical properties of temperature fluctuations etc.

The aim of the present investigation is to elucidate the instantaneous and average temperature fields on

* Corresponding author. Tel.: +972-48-292-058; fax: +972-48-343-362.

E-mail address: hetsroni@tx.techion.ac.il (G. Hetsroni)

0017-9310/99/$ - see front matter
PII: S0017-9310(99)00041-1

Nomenclature

b	the width of the channel
c_p	specific heat of the fluid at constant pressure
d	the diameter of the cylinder
d_B	the diameter of the particle in the lattice
D	the diameter of the pipe
f	the friction factor
h	the local heat transfer coefficient
H	the depth of the fluid layer
Nu	the Nusselt number
Pr	the Prandtl number
q	heat flux
Re_H	the Reynolds number based on fluid's depth
Re_θ	the Reynolds number based on the momentum thickness
Re_D	the Reynolds number based on the pipe diameter
T_w	the temperature of the wall
T'_w	the fluctuations of the temperature on the wall
T_f	the temperature of the fluid
u	mean flow velocity
u^+	dimensionless streamwise velocity
u'	the fluctuations of the flow velocity
u^*	friction velocity
x, y	longitudinal and vertical Cartesian coordinates
y^+	dimensionless distance normal to the lower wall
x^+	dimensionless longitudinal coordinate
$\bar{x}$	dimensionless longitudinal coordinate normalized to diameter of cylinder

Greek symbols

ϵ_u	the intensity of velocity fluctuations
ϵ_T	the intensity of wall temperature fluctuations
Λ	the spacing between the thermal streaks
Λ^+	non-dimensional spacing between the thermal streaks
λ	the thermal conductivity of the fluid
ν	kinematic viscosity
ρ	the density of the fluid

the surfaces of smooth and rough walls in developed turbulent channel and pipe flows, as well as the effect of macroscale roughness on the heat transfer intensity.

It is our contention that the temperature distribution on the wall, as measured by our heated foil technique, is a signature of the velocity distribution in the boundary layer of the turbulent flow. A high temperature streak can be interpreted as a result of low velocity near the wall, and vice versa. Therefore, the study of various characteristics of the temperature distribution on the wall leads to better understanding of the velocity distributions in the boundary layer of turbulent flow.

The time and space behavior of the temperature distribution were recorded, and are available upon request.

2. Experimental set-up

2.1. Equipment

To study the temperature fields on the smooth and rough walls in a wide range of Reynolds numbers, two experimental set-ups were used: a flume and a pipe. The first of them was described by Hetsroni and Rozenblit [16], therefore, presented here is only the main features of the test section and the scheme of measurement (Fig. 1(a)). The flow loop consisted of a stainless steel open flume 4.3 m long, 0.32 m wide and 0.1 m deep. Water at constant temperature was recirculated within the flume. The test section was located at a distance 2.5 m from the channel entrance, where a developed flow was established. The constantan heater

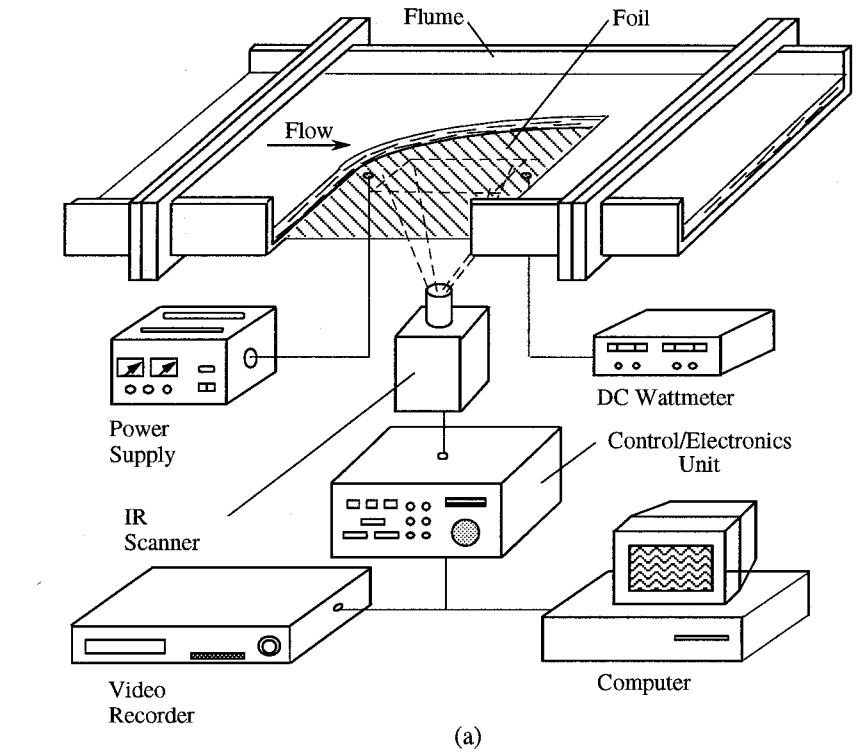

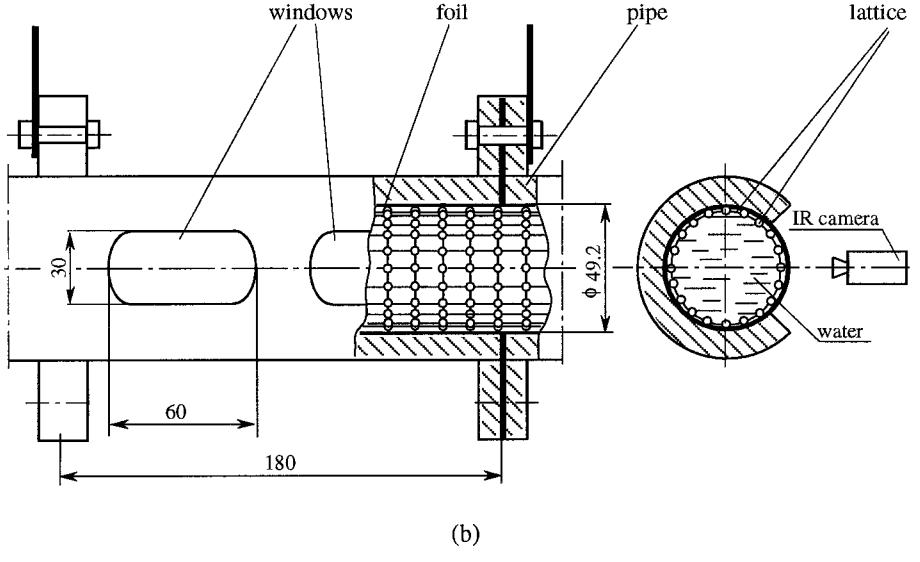

Fig. 1. The schemes of test section: (a) open channel flow; (b) pipe flow.

(on an insulated frame) was made of a foil 0.33 m long, 0.2 m wide and 50 μm thick. The window of the frame was 0.3 m long and 0.15 m wide. The foil was attached to the window by means of contact adhesive and was coated on the airside, by black mat paint of about 20 μm thickness. Constant heat flux from the

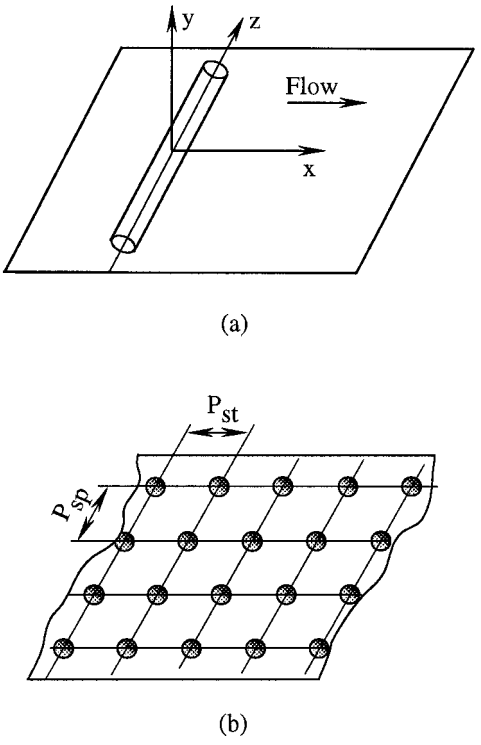

Fig. 2. Macro-scale roughness: (a) cylinder; (b) lattice of spherical particles.

wall was achieved by supplying DC power up to 300 A, to the foil.

The flow depth H ranged from 0.037 m to 0.058 m. The cross-sectional mean velocity ranged from 0.15 m/s to 0.23 m/s, so that the Reynolds number, based on the momentum thickness was $Re_\theta = 300$–600. A fully developed flow was established in the region beyond 2.5 m downstream from the inlet to the flume, which was confirmed by the measurements of both the velocity profile and distributions of root-mean-square (RMS) values of streamwise velocity fluctuations u'. The measurements were performed at the centerline of the flume, i.e. at $z = 0$ (z is the spanwise direction). Velocity measurements were done by means of a hot film anemometer. The standard 90° conical probe was connected to a traversing mechanism having a spatial resolution of 10 μm. The anemometer signal was transmitted in digital code through an acquisitor to a PC. The hot-film probe was calibrated in the water flume, and after calibration the sensor was positioned in the boundary layer and the data were recorded. The calibration was re-checked periodically. When the sensor drifted from the previous calibration more than 2%, the data were rejected and the calibration process was repeated. The uncertainty in a single measurement of the streamwise velocity is estimated to be of the order 2–4%; the highest value corresponds to the lowest velocity. Note, that such accuracy is typical for the hot-film measurements of mean velocity [17], whereas it is about 8% for the measurements of turbulent fluctuations.

The experimental set-up to study heat transfer in a pipe flow was made of plastic tube 49 mm in diameter. It consists of five sections: (i) calming; (ii) flow development (3.6 m long); (iii) pressure measurement (1.2 m long); (iv) test; and (v) outlet. The heated surface of the test section was made of constantan foil 0.18 m long and 50 μm thick glued to the inner wall of the plastic tube. The windows of the test section are 0.06 m long and 0.03 m wide. The heated section can be rotated around the horizontal axis to put the windows in a desired position. The flow was produced by a cen-

Table 1
The general parameters of the experimental set-ups

Item		Unity	Channel	Pipe		
Characteristic dimensions	H	$m \times 10^{-3}$	37–58	–		
	D	$m \times 10^{-3}$	–	49.2		
Mean water temperature	$\bar{T}_f$	°C	20 ± 0.1	20 ± 0.1		
Mean flow velocity	u	$m\ s^{-1}$	0.15–0.23	0.40–1.37		
Reynolds number	Re_H		5500–8700	–		
	Re_D		–	20000–68600		
Heat flux	q	$W\ m^{-2}$	2700–10000	18000–41000		
Roughness type			Single cylinder	Lattices of spherical particles		
				N1	N2	N3
Cylinder diameter	d	$m \times 10^{-3}$	4.0			
Particle diameter	d_B	$m \times 10^{-3}$	–	5	3.9	2.7
Pitch in the streamwise direction	P_{st}	$m \times 10^{-3}$	–	35	15	11
Pitch in the spanwise direction	P_{sp}	$m \times 10^{-3}$	–	8	7	6

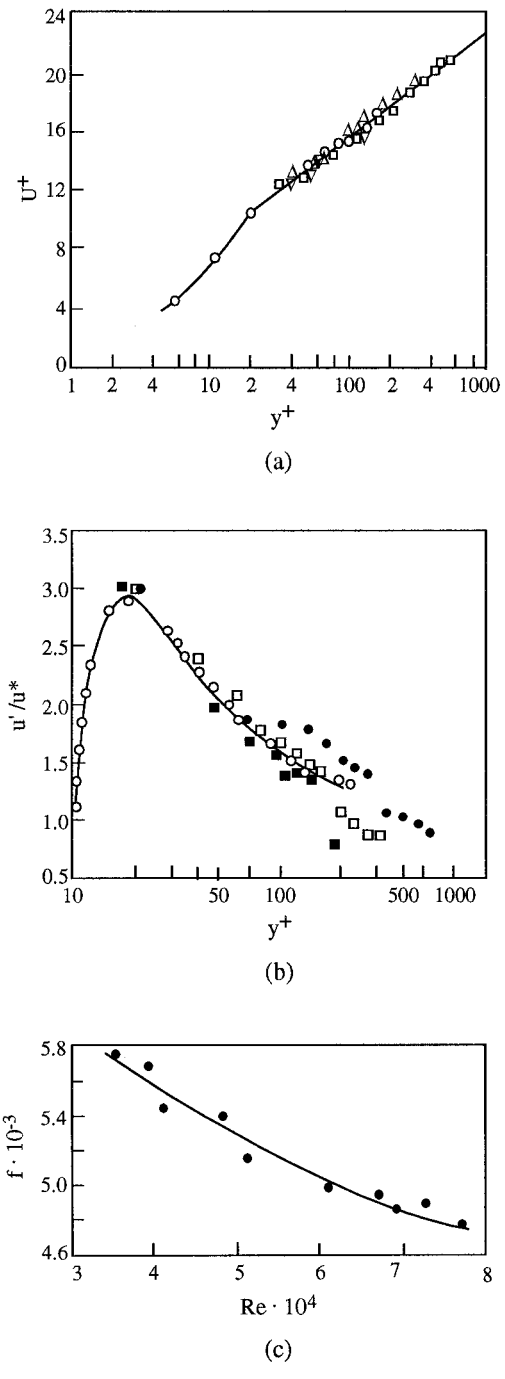

Fig. 3. The distribution of mean and fluctuation velocities near the wall (channel flow). (a) The log–law plot of mean velocity profiles over smooth wall: —, $u^+ = 2.5\ln y^+ + 5$; ∇, $Re_\theta = 300$; Δ, $Re_\theta = 470$; □, $Re_\theta = 600$; ○, data by Antonia et al. [22]. (b) Distribution of dimensionless streamwise turbulence intensities near the wall: ■, $Re_\theta = 300$; □, $Re_\theta = 470$; ●, $Re_\theta = 600$; ○, data by Nishino and Kasagi [24]. (c) Dependence of friction factor $f = 2\tau/\rho u^2$ on the Reynolds number. ●, experimental data; —, Blasius equation.

trifugal pump and was measured by means of a flowmeter.

A number of heat transfer and hydrodynamic verification runs were undertaken prior of the data logging. A series of pressure drop tests was made to establish that the flow behaves as a fully developed one. The pressure drop was measured across 1100 mm length by pressure transducers. The upstream point of measurements was 74 tube diameters from the entrance to the development section. The pressure drop results agree with the accepted smooth pipe values (Blasius equation). The standard deviation does not exceed 2% for all data sets.

Two types of macro-scale roughness (Fig. 2(a,b)) were used to disturb the flow: (i) a single cylinder ($d = 4.10^{-3}$ m), placed on the wall and oriented in the spanwise direction (the first set-up); (ii) the lattices of spheroidal particles of different sizes (the second set-up). The parameters of the lattices used here are presented in Table 1.

2.2. Temperature field diagnostics

To study temperature fields on the walls the hot-foil infrared technique (HFIRT) was used. Such technique has been applied to explore various thermal and hydrodynamic problems [16,11,18,19]. Hetsroni et al. [20] have shown that HFIRT allowed to obtain detailed information on the wall temperature, in particular, temperature fluctuations.

The IR radiometer was used to measure average and fluctuation temperatures. It consists of a scanner and control/electronics unit. The scanner incorporates electro-mechanical servos to perform horizontal and vertical scanning. Horizontal scanning is performed at a 4 kHz rate in a resonant (sinusoidal) mode. Vertical scanning is performed using a sawtooth pattern commensurate with standard television formats. The control/electronics unit contains circuits to process, digitize and reformat the IR signal or display it colored or black and white on the display or external video monitor.

The temperature range of the measurements of the IR radiometer is −20–1500°C, with a minimum detectable temperature difference of 0.1°C at 30°C. Through calibration, the radiometer is very accurate in a narrow temperature range, giving the typical noise equivalent temperature difference only, which is less than 0.2°C (with image average less than 0.05°C). A typical horizontal resolution is 1.8 mrad or 256 pixels/line. The range of ambient operating temperatures of the IR radiometer is −15–+50°C. The scanner of the IR radiometer was situated at a distance of about 0.5 m from the heated foil. The calibration of the IR imaging radiometer was checked in the special device with a precision mercury thermometer placed in the water.

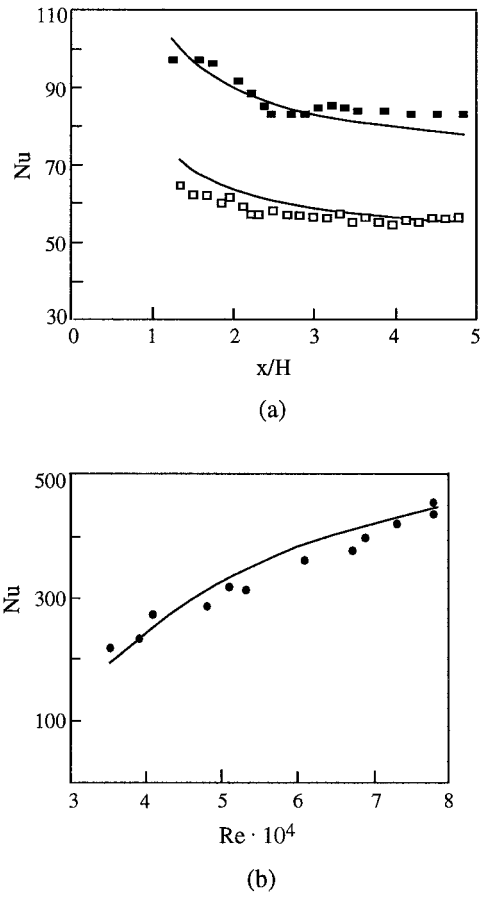

Fig. 4. Heat transfer coefficient. (a) Open channel flow experimental data: ■, $Re=5500$, □, $Re=8500$; —, the theoretical prediction by Kays [2]. (b) Pipe flow: ●, experimental data; —, theoretical prediction by Deissler [25].

The Inframetrics model 760 operates with individual Mercury/Cadmium/Telluride detector. It is cooled by Inframetrics integrated cooler to 77 K for maximum thermal sensitivity and high spatial resolution. The frequency response of IR radiometer is 25 frames $\times$ s^{-1}.

The accuracy of the IR radiometer (manufacturer data) was $\pm 2\%$. The heat flux (DC power) was determined with an accuracy of 0.5%. The water depth and flow velocity were determined with accuracy of $\pm 0.5\%$ and 2%, respectively. The water temperature was measured by means of a precision mercury thermometer with an accuracy of $\pm 0.05^{\circ}$C. The errors in the Reynolds number did not exceed 2.6%. The accuracy of the estimation of the non-dimensional spacing of the thermal streaks was 16%.

The frequency response of heated foil was estimated according to the work by Hetsroni et al. [20]. It was found that foil characteristic frequency did not exceed 10 s^{-1}.

2.3. Characteristics of the flows

The profiles of mean velocity at $300 < Re_\theta < 600$ (Re_θ is the momentum thickness Reynolds number) are depicted in Fig. 3(a). The solid line on this graph corresponds to the logarithmic law $u^+ = 2.5y^+ + 5.0$ ($u^+ = u/u^*$, u and u^* are the local and friction velocities, respectively). The profiles of velocity were fitted to this line by adjusting u^* so that the experimental values of $u+$ and y^+ agreed with the 'law of the wall'. The present velocity distribution and the friction velocity u^* are in agreement with the measurements by Rashidi et al. [21] and Kaftori et al. [22], who used an identical flume. In Fig. 3(a) the data by Antonia et al. [23] are also presented. It is seen that these results agree fairly well with the data of the present experiments. In both cases, the dependence $u^+ = 2.5y^+ + 5.0$ is fairly much within the limits $20 < y^+ < 600$. Note, that the lowest $Re_\theta = 300$ in our experiments seems to be the minimum Reynolds number at which turbulent flow is maintained [24].

The turbulence intensity distributions in a flume are shown in Fig. 3(b). For comparison, the experimental data by Nishino and Kasagi [25] are also presented in this graph. The u'/u^* profiles exhibit a clear Reynolds number dependence. For $y^+ > 20$ the value of u'/u^* decreases less rapidly with increasing Reynolds number. However, the latter practically does not affect the shear stress distribution [23].

Some results related to hydraulic characteristics of the second set-up are plotted in Fig. 3(c). These data agree fairly well with known results on the friction in smooth pipes.

The data of the thermal tests of the first and the second experimental set-ups are presented in Fig. 4(a,b). Here are also shown the results of the heat transfer coefficient calculation in accordance with Kays [2] and Deissler [26]. In both cases (flume and pipe flows) a fairly good agreement between experimental and calculated data are observed. The general parameters of the first and the second experimental set-ups are presented in Table 1.

3. Results and discussion

3.1. Macro-scale thermal structure

Appearance of the macro-scale thermal structures on the wall in a turbulent flow was observed [27,28,16,13]. These structures (so-called thermal streaks) were oriented mainly in the streamwise direction. They move slowly in the downstream direction and meander about in the lateral direction. The thermal streaks movement is accompanied by some twisting and merging with the neighbouring streaks.

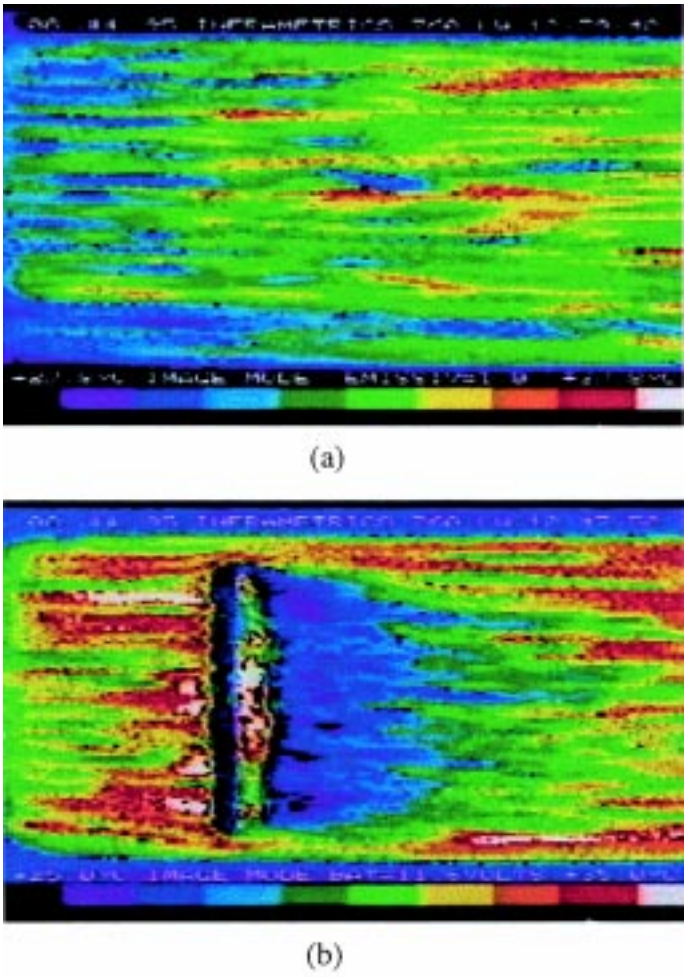

Fig. 5. Temperature field on the wall (open channel flow; flow is from the left to the right): (a) smooth surface, $Re_H = 8500$; (b) rough surface, $Re_H = 8500$.

The existence of thermal streaks demonstrates the heterogeneity of the temperature distribution on the wall. The typical temperature fields on the smooth and rough walls are shown in Figs. 5 and 6. It is seen that the number of thermal streaks, in the streamwise direction in the unperturbed flume and pipe flows, is practically constant (Figs. 5(a) and 6(a)). The measurements show that the dimensionless spanwise thermal streak spacing $\Lambda^+ = \Lambda u^*/\nu$ (Λ is a dimensional spanwise streak spacing, ν is the kinematic viscosity) is about $\Lambda^+ \approx 90$. This result agrees with the data by Kline et al. [17], Achia and Thompson [29], Iritani et al. [27], Smith and Metzler [30], Oldaker and Tiederman [31] on hydrodynamic and thermal structures of the near-wall flow.

However, notice that the temperature field is drastically changed on the roughened wall, Fig. 5(b). An existence of a macro-scale roughness leads to the total disruption of the thermal streaky structure behind the obstacle. In the wake of the disturbance, the streaky structure disappears, while further downstream the regular thermal streaky structure once again is restored [12,13].

The structures of the temperature field over the pipe wall with roughness in the form of lattices of spherical particles are shown in Fig. 6. In these pictures, the infrared images of instantaneous thermal fields of the heated wall are presented. Fig. 6(a) shows a temperature field of the pipe wall without a lattice. A typical instantaneous streaky structure over the wall can be seen here. Fig. 6(b) shows the infrared image of the heated wall in the case that the lattice N1 is inserted into the pipe. It can be seen that the color play is shifted towards a lower wall temperature, i.e. the heat transfer coefficient increases. The color play of Fig. 6(c) corresponds to the lowest temperature level, (in

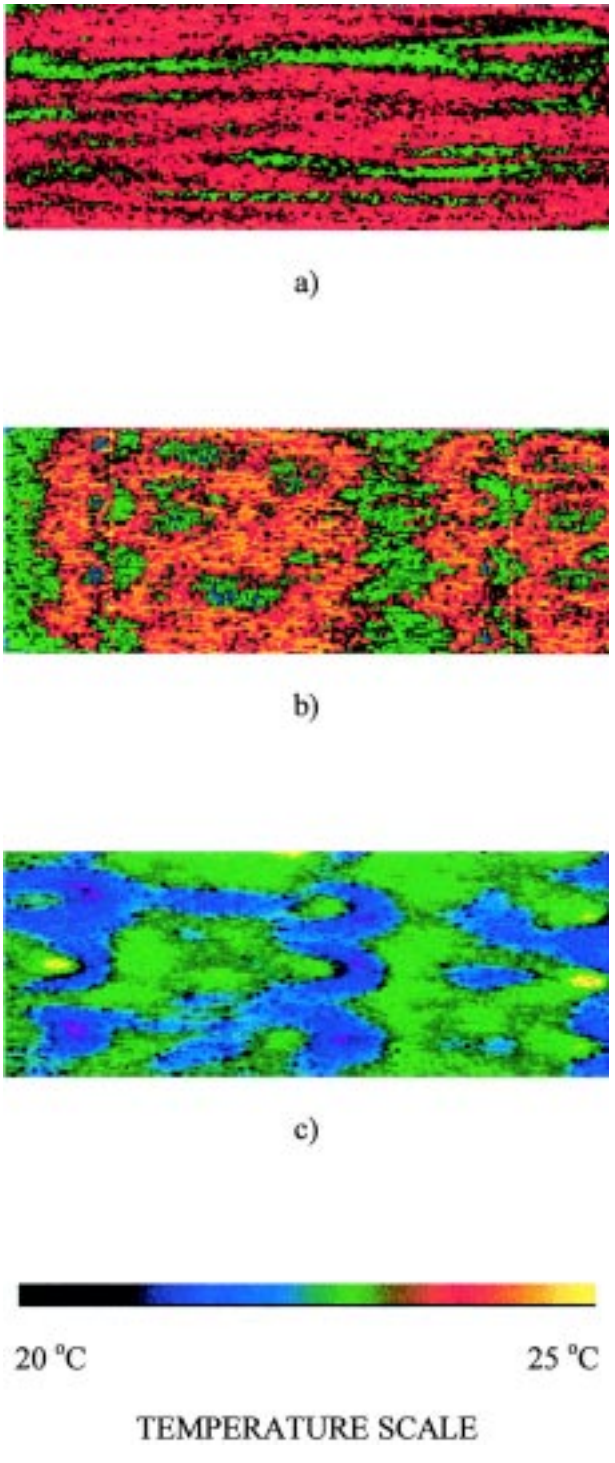

Fig. 6. Temperature field on the wall (pipe flow): (a) smooth wall; (b) lattice 1 (Table 1); (c) lattice 3 (Table 1).

this case the lattice N3 was mounted). There are only small 'islands' of relatively high temperature, since the flow is completely disturbed by the disturbances in the lattice. In the figures with lattice roughnesses, two zones of a decreased temperature field were observed. The first of them is located underneath and in front of each particle and the second one is revealed in the wake behind it with the length of about $4d_b$. The measurements showed that the location of the second zone weakly depends on the Reynolds number. Similar observations were done by Hetsroni et al. [12] with a single particle. In that work, experimental observations and numerical simulations showed that there is a cool region in front, and under, the particle, and another cold region in its wake.

The above-mentioned results reveal some characteristics of instantaneous temperature fields on smooth and rough walls. Some features of the average temperature fields are now briefly considered. First of all the data characterizing macro-scale structure of these fields are presented:

Use RMS_T of the lateral temperature distribution as a measure of average temperature variations in a given cross section, i.e.

$$RMS_T = \sqrt{\frac{1}{n}\sum_{i=1}^{n}[T_w(z) - \bar{T}_w(z)]^2} \quad (1)$$

where $T_w(z)$ and $\bar{T}_w(z)$ are the instantaneous and average temperatures at a given point and a given cross section, respectively, n is a number of points of measurements.

The dependencies $RMS_T(t_{av})$ (t_{av} is the averaging time) for 3 cross sections far enough from the leading edge of the heated foil, on the integration time are plotted in Fig. 7. These data are obtained by image processing of 400 pictures with a time step of 0.1 s. They show that the level of variations in the temperature field decreases with increasing of averaging time. This effect leads to smoothing of the temperature field due to migration of thermal streaks in spanwise direction. Homogeneity of the temperature field at large t_{av} shows that the probability of thermal streaks appearing at any particular region of the wall is the same. This is a rather important observation, pointing at the random nature of the phenomena, i.e. the appearance of the coherent structure on the wall looks like a random process.

3.2. Temperature fluctuations

The near wall region of the turbulent flow possesses a very complicated structure which is a consequence of the interaction of vortices of various scales [32–35]. Coherent structures (bursting, ejections etc.) play an

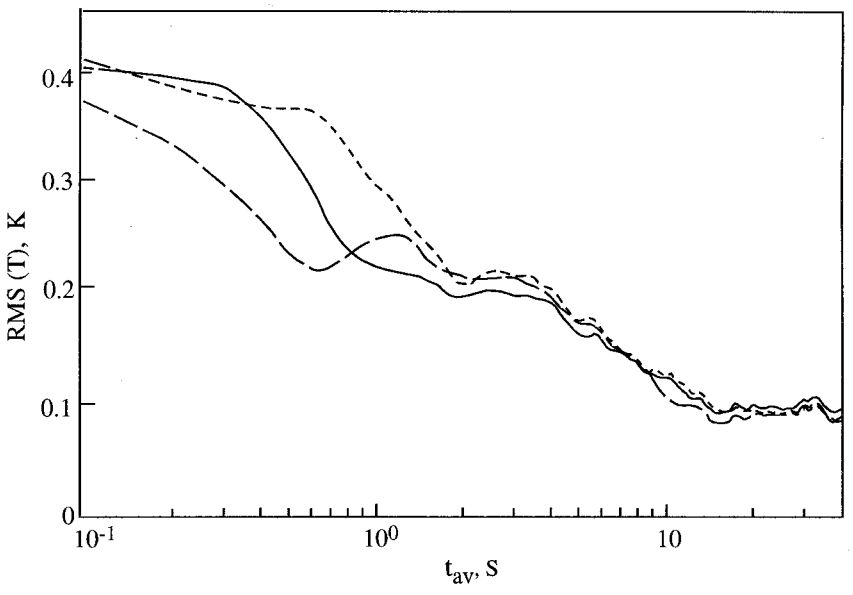

Fig. 7. The dependences $RMS_T(t_{av})$ for $Re_H = 8500$ along line (for 3 cross sections): —, $x^+ = 1000$; ..., $x^+ = 2000$; - - -, $x^+ = 3000$.

important role in the turbulence production and heat transfer. The transversal motion of the fluid due to bursting process leads to penetrating of the cold fluid from the external to near wall region, sublayer breakdown, formation of zones with very small thermal resistance and abrupt change of wall temperature in the vicinity of the burst/wall impact point. Although the turbulence/wall interaction is the reason for wall temperature fluctuations, their characteristics depend not only on the hydrodynamics of the near wall flow but also on physical properties of the wall material. These considerations were used by Hetsroni et al. [20] to estimate the intensity of temperature fluctuations on the wall in a turbulent flow. The authors assumed that due to the fluid/wall interactions a temperature heterogeneity (thermal spot) was formed on the wall.

The model of the thermal spot appearance allows one to determine the behavior of temperature fluctu-

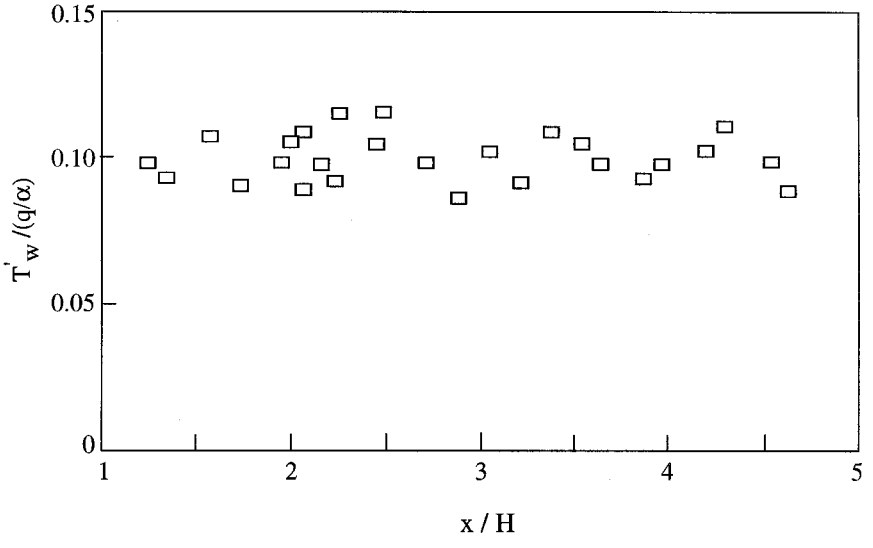

Fig. 8. The dependence $T'_w/(q/\alpha)$ vs x/H (channel flow). $Re = 8500$; $q = 1 \times 10^4$ W/m^2.

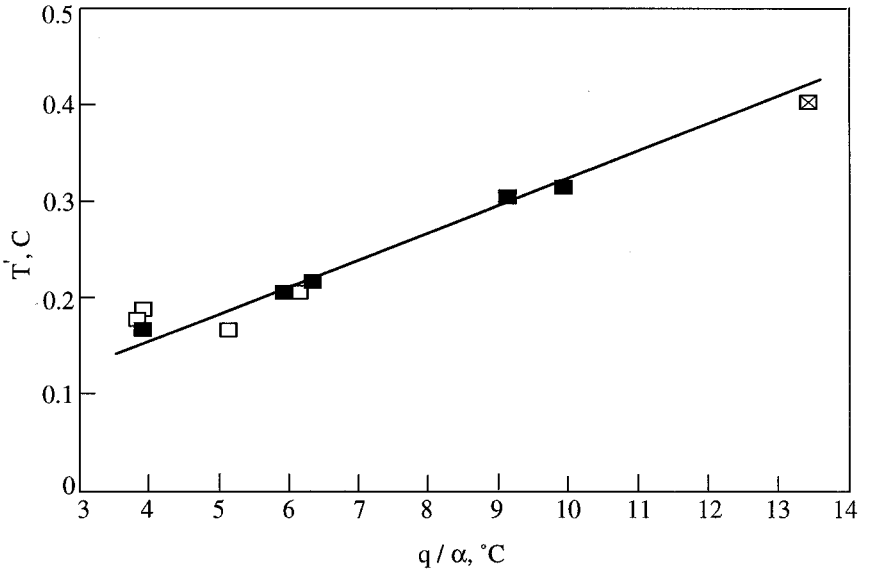

Fig. 9. The dependence T'_w vs q/α at various heat flux q. □, $q=1.78\times10^4$ W/m^2; ■, $q=2.75\times10^4$ W/m^2; ⊠, $q=2.1\times10^4$ W/m^2: $20{,}000 \le Re \le 68{,}500$.

ations, depending on the intensity of velocity fluctuations, physical properties of wall material as well as the heat transfer. For the simplest type of flow disturbances (harmonic fluctuations of velocity) Hetsroni et al. [20] obtained the expression for the intensity of the temperature fluctuation on the wall, i.e.:

$$T' = \frac{S_o u'}{1+\omega^2 M^2} \tag{2}$$

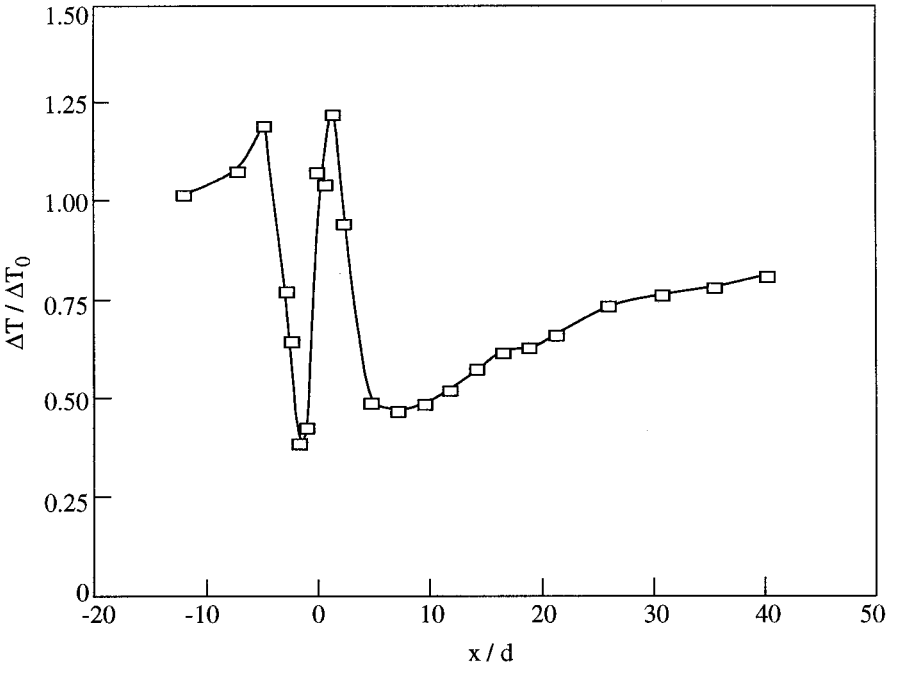

Fig. 10. The dimensionless first moment of the wall temperature vs x/d.

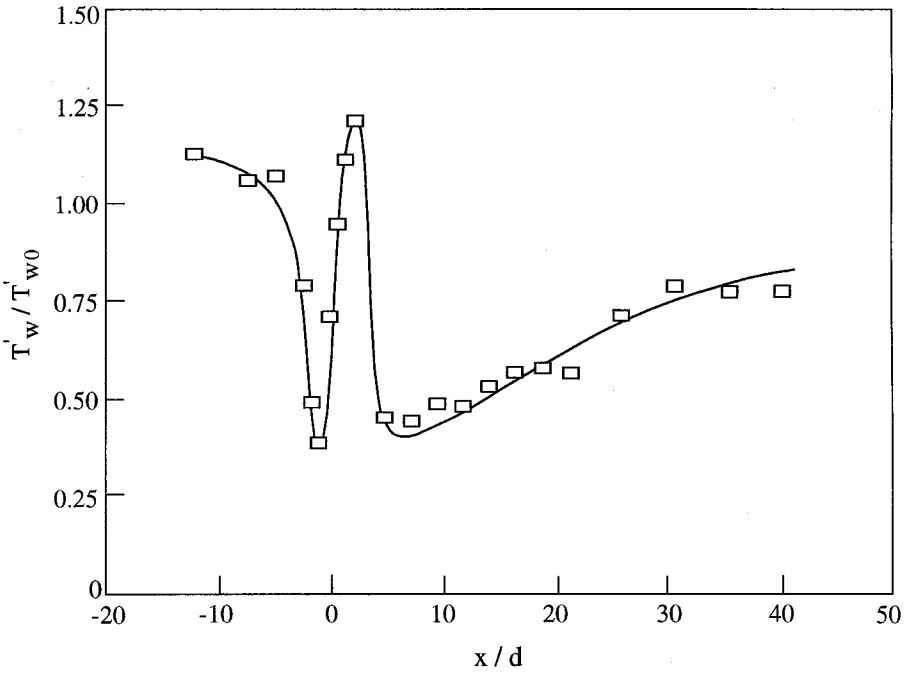

Fig. 11. The level of the dimensionless temperature fluctuations vs x/d.

where

$$S_o = \frac{1}{\alpha(\bar{u})\varphi}(\bar{T}_w - T_f)\frac{d\alpha(\bar{u})}{d\bar{u}}, \quad M = \frac{\rho c \delta}{\alpha(\bar{u})\varphi},$$

$\alpha(\bar{u})$ is the heat transfer coefficient, $\bar{u}$ is the mean flow velocity, T_w is the mean temperature, T_f is the fluid temperature, u' are the velocity fluctuations, ρ, c are density and specific heat of the foil material, respectively, δ is the wall thickness, $\varphi \approx 1$ is a parameter, ω is a characteristic frequency.

Eq. (2) has the following form (for a thin foil):

$$T' = \frac{u'}{\alpha(\bar{u})}(\bar{T}_w - T_f)\frac{d\alpha(\bar{u})}{d\bar{u}} \tag{3}$$

Then, taking into account that $Nu = A\ Re^n\ Pr^m$, where Nu and Pr are the Nusselt and Prandtl numbers; A, m, n are known constants, Eq. (3) can be rewritten as

$$T'_w = \frac{u'}{u} n \frac{q}{\alpha} \tag{4}$$

where q is the heat flux on the wall.

Thus, in the hydrodynamic stabilized flow the temperature fluctuations are directly proportional to the heat flux value and inversely proportional to the heat transfer coefficient.

In the developed channel flow the intensity of velocity fluctuations does not change downstream [36]. Accordingly, with (4), the intensity of the temperature fluctuations must be constant downstream at a given Reynolds number. It can be seen that Eq. (4) agrees fairly well with the experimental data (Fig. 8).

In Fig. 9 the change of temperature fluctuations T'_w is shown vs q/α at various values of heat flux q and Reynolds number in a pipe flow. In spite of the significant scatter of experimental points, these data also support Eq. (4).

3.3. Statistical characteristics

Statistical characteristics of temperature fields on the surface of smooth and rough walls were determined by averaging instantaneous temperatures in a given point during some time interval. The latter was chosen so that the results of the statistical analysis did not depend on t_{av}.

The mean temperature distribution along the foil with a single macro-scale cylindrical roughness is plotted in Fig. 10. It is seen that the cylinder leads to sharp changes in the temperature field as compared with the undisturbed flow. The temperature distribution has two minima located in front and behind the cylinder. In front of a single cylinder one can see a sharp decrease of mean temperature. At the distance $x/d = -1$ the minimum $\Delta T/\Delta T_o$ is observed. Then mean temperature increases up to $\Delta T/\Delta T_o = 1.2$. At $x/d > +1$ a sharp temperature drop takes place. The second minimum $\Delta T/\Delta T_o$ is located at $x/d \sim 5$. Far

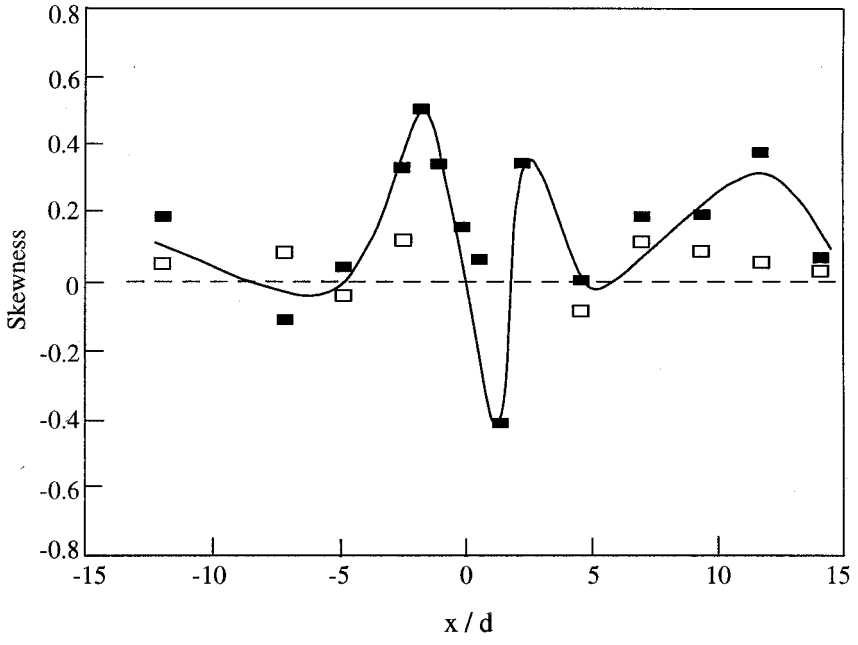

Fig. 12. Skewness depending on dimensionless distance from cylindrical roughness: □, smooth wall; ■, with cylinder.

from the cylinder temperature increased to its level in the undisturbed flow.

The distribution of the wall temperature fluctuations in the vicinity of a cylindrical roughness is shown in Fig. 11. It is seen that this distribution is similar to the mean temperature distribution. In both cases the

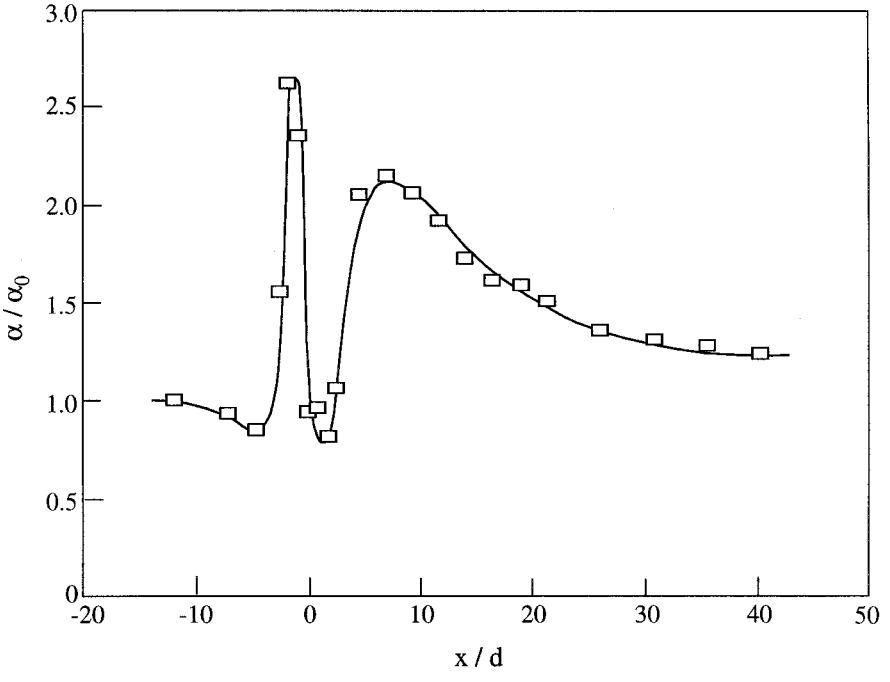

Fig. 13. The distribution of the dimensionless heat transfer coefficient vs x/d.

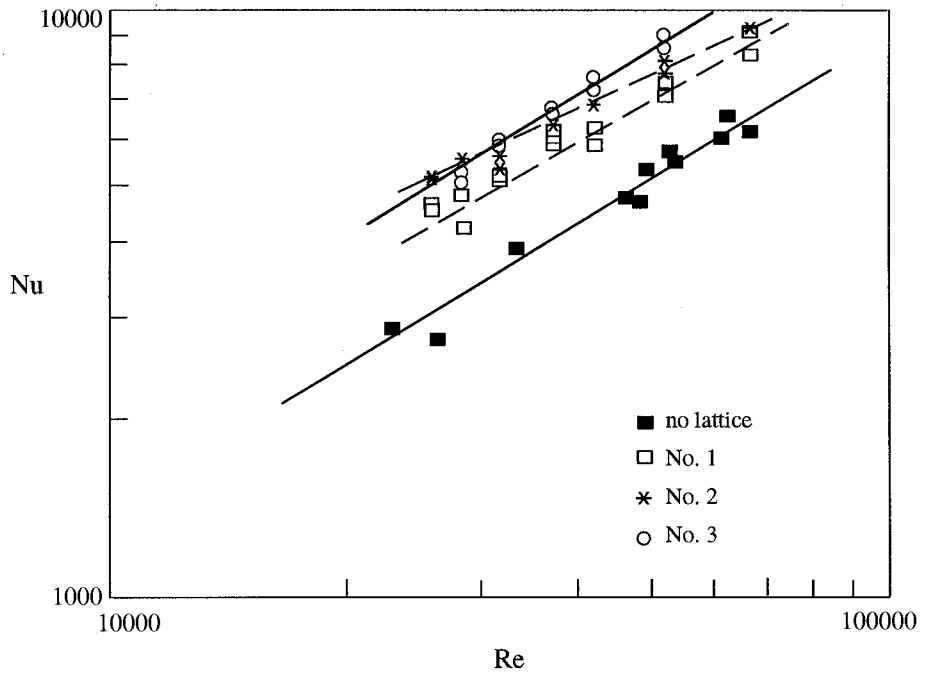

Fig. 14. The heat transfer enhancement by the lattice

dependencies $\Delta T/\Delta T_o = f(x/d)$ and T'_w/T'_{wo} have characteristic extrema located in front of and behind the macro-scale disturber.

The dependence of skewness on the dimensionless distance is illustrated in Fig. 12. It is seen that the skewness value is close to zero for the smooth surface (normal distribution). In contrast, the value of skewness is quite different from zero for a rough surface. According to the data in Fig. 12, the temperature fluctuations distribution on the rough wall is not normal.

3.4. Heat transfer coefficient

The distribution of the dimensionless heat transfer coefficient α/α_o in the vicinity of the cylindrical disturber is presented in Fig. 13. The single macro-scale roughness leads to a strong modulation of the flow. As a consequence a sharp change of heat transfer coefficient near the disturber occurs. The change of α/α_o vs the distance downstream has two maxima in the regions of a direct interaction between the cold water from bulk flow and the wall, and single minimum in the stagnation zone, behind the cylinder. At the first maximum heat transfer is enhanced three times. A similar effect, a significant heat transfer enhancement in front of the body was observed at some other types of macro-scale roughness: coarse spherical particle, square or circular columns [37,38].

The effect of macro-scale roughness on the heat transfer in a pipe flow is illustrated in Fig. 14. It is seen that macro-scale roughness in the form of a lattice of spherical particles leads to a remarkable enhancement of the heat transfer coefficient. This effect depends on various parameters of the lattice and can reach 200–300% in comparison with undisturbed flow (the optimal values of pitches are: 1.5–3d_b for the spanwise direction and 3–5d_b for the streamwise one).

4. Conclusions

The temperature fields over the smooth and rough walls, at the developed turbulent flow in the open channel and pipe were studied by using infrared thermography. It is shown that the instantaneous temperature field on the heated walls possesses a streaky structure, whereas the average temperature fields are practically uniform. The measurements show that the intensity of temperature fluctuations, on the surface of a smooth wall, is directly proportional to the heat flux from the wall and inversely proportional to the heat transfer coefficient. Macro-scale roughness on the wall (a single cylinder, lattice of spherical particles) leads to destruction of the thermal streaky structure. This process is accompanied by a sharp transformation of average and fluctuations temperature fields and increasing of heat transfer coefficient by 200–300%.

Acknowledgements

This research was supported by the Technion VPR fund; Miami Energy Research Fund; the Fund for the Promotion of Research at the Technion. A. Mosyak and R. Rozenblit are partially supported by the Center for Absorption in Science, Ministry of Immigrants Absorption, State of Israel, L. P. Yarin is supported by the Israel Council for Higher Education.

References

[1] H. Grober, S. Erk, U. Grigull, Die Grundgesetze der Warmeübertragung, Springer, Berlin, 1955.
[2] W.M. Kays, Convective Heat and Mass Transfer, McGraw-Hill, New Jersey, 1966.
[3] A. Bejan, Convection Heat Transfer, Wiley, New York, 1984.
[4] A. Zukauskas, High-Performance Single-Phase Heat Exchangers, Hemisphere, New York, 1989.
[5] R.I. Webb, Principles of Enhanced Heat Transfer, Wiley, New York, 1994.
[6] J.C. Han, Heat transfer and friction in channels with two opposite rib-roughness walls, ASME Journal of Heat Transfer 104 (1984) 774–781.
[7] J.C. Han, S. Ou, J.S. Park, C.K. Lei, Heat transfer enhancement in channels with turbulent promoters, ASME Journal of Engineering for Gas Turbines and Power 107 (1985) 628–635.
[8] D.E. Metzger, C.S. Fan, Y. Yu, Effect of rib angle and orientation on local heat transfer in square channels with angled roughness ribs, in: Compact Heat Exchangers, Hemisphere, New York, 1990, pp. 151–167, A Festschrift for A.L. London.
[9] M. Hishida, K. Takase, Heat transfer coefficient of the rubber surface, Proceeding of the ASME/JSME. Thermal Engineering Conference 3 (1991) 100–103.
[10] M. Hirota, H. Fujita, Y. Yokosawa, Experimental study of convective heat transfer for turbulent flow in a square duct with a ribbed rough (characteristics of mean temperature field), ASME J. Heat Transfer 116 (1994) 332–340.
[11] D.A. Aliaga, J.P. Lamb, D.E. Klein, Convective heat transfer distributions over plates with square ribs from infrared thermography measurements, Int. J. Heat Mass Transfer 37 (1994) 363–374.
[12] G. Hetsroni, R. Rozenblit, D.M. Lu, Heat transfer enhancement by a particle on the bottom of a flume, Int. J. Multiphase Flow 21 (1995) 963–984.
[13] G. Hetsroni, A. Mosyak, L.P. Yarin, Thermal streaks regeneration in the wake of a disturbance in a turbulent boundary layer, Int. J. Heat Mass Transfer 40 (1997) 4161–4168.
[14] N. Kasagi, A. Kuroda, M. Hirata, Numerical investigation of near-wall turbulent heat transfer taking into account the unsteady heat conduction in the solid wall, ASME J. Heat Transfer 111 (1989) 385–392.
[15] T.P. Sommer, R.M.C. So, H.S. Zhang, Heat transfer modeling and the assumption of zero wall temperature fluctuations, ASME J. Heat Transfer 116 (1994) 855–863.
[16] G. Hetsroni, R. Rozenblit, Heat transfer to liquid–solid mixture in a flume, Int. J. Multiphase Flow 20 (1994) 671–689.
[17] S.J. Kline, W.C. Reynolds, F.A. Schraub, P.W. Runstadler, The structure of turbulent boundary layer, J. Fluid Mech 30 (1967) 741–773.
[18] H. Lee, D.E. Klein, J.P. Lamb, Constant flux, turbulent convection data using infrared imaging, Int. J. Heat Mass Transfer 37 (1994) 535–539.
[19] G.M. Carlomagno, Infrared thermography and convective heat transfer. Experimental heat transfer, fluid mechanics and thermodynamics, Proceedings of the Fourth World Conference on Experimental Heat Transfer, Fluid Mechanics and Thermodynamics 1 (1997) 29–41.
[20] G. Hetsroni, R. Rozenblit, L.P. Yarin, A hot-foil infrared technique for studying the temperature field of a wall, Measurement Science and Technology 7 (1996) 1418–1427.
[21] M. Rashidi, G. Hetsroni, S. Banerjee, Particle turbulence interaction in a boundary layer, Int. J. Multiphase Flow 16 (1990) 935–949.
[22] D. Kaftori, G. Hetsroni, S. Banerjee, Funnel shaped vortical structures in wall turbulence, Phys. Fluids A.6 (1994) 3035–3050.
[23] R.A. Antonia, M. Teitel, J. Kim, L.W.B. Browne, Low-Reynolds number effects in a fully developed turbulent flow, J. Fluid Mech. 236 (1992) 579–605.
[24] J.H. Preston, The minimum Reynolds number for a turbulent boundary layer and the selection of a transition device, J. Fluid Mech. 3 (1958) 373–384.
[25] K. Nishino, N. Kasagi, Turbulence statistics measurements in a two-dimensional channel flow using a three-dimensional particle tracking velocimeter, Proceedings of the Seventh Symposium on Turbulent Shear Flows, Stanford 2 (1989) 22.1.1–22.1.6.
[26] R.G. Deissler, Turbulent heat transfer and friction in the entrance regions of smooth passages, Trans. ASME 77 (1955) 1221–1233.
[27] Y. Iritani, N. Kasagi, M. Hirota, Heat transfer mechanism and associated turbulence structure in the near-wall region of a turbulent boundary layer, Turbulent Shear Flow IV (1983) 223–234.
[28] J.C. Simonich, R.S. Moffat, New technique for mapping heat transfer coefficient contours, Rev. Sci. Instrum. 53 (1982) 678–683.
[29] B.U. Achia, D.W. Thompson, Structure of the turbulent boundary layer in drag-reducing pipe flow, J. Fluid Mech. 81 (1977) 439–464.
[30] C.R. Smith, S.P. Metzler, The characteristics of low-speed flow streaks in the near-wall region of a turbulent boundary layer, J. Fluid Mech. 129 (1985) 27–54.
[31] D.K. Oldaker, W.G. Tiederman, Spatial structure of the viscous sublayer in drag reduction channel flow, Phys. Fluids 20 (1975) 133–144.
[32] A.A. Townsend, The Structure of Turbulent Shear Flow, Cambridge University Press, Cambridge, 1976.
[33] S.J. Kline, The role of visualization in the study of the

structure of the turbulent boundary layer, in: C.R. Smith, D.E. Abbot (Eds.), Coherent Structure of Turbulent Boundary Layers, AFOSR, Lehigh, 1978, pp. 1–26.

[34] B.J. Cantwell, Organized motion in turbulent flow, Ann. Rev. Fluid Mech. 13 (1981) 457–515.

[35] M. Gad-el-Hak, P.R. Bandyopadhyay, Reynolds number effects in wall-boundary turbulent flows, Appl. Mech. Rev. 47 (1994) 307–365.

[36] G. Comte-Bellot Ecoulement turbulent entre deux parois paralleles. Edite par le service de documentation scientifique et technique de l'armement, Paris, 1965.

[37] G. Hetsroni, R. Rozenblit, L.P. Yarin, The effect of coarse particles on the heat transfer in a turbulent boundary layer, Int. J. Heat Mass Transfer 9 (1997) 2201–2217.

[38] X. Zhang, J. Stasiek, M.W. Collins, Experimental and numerical analysis of convective heat transfer in turbulent channel flow with square and circular columns, Experimental Thermal and Fluid Science 10 (1995) 229–237.